A THREE-DIMENSIONAL TURBINE ENGINE ANALYSIS COMPRESSOR CODE (TEACC) FOR STEADY-STATE INLET DISTORTION*

Alan Hale
Sverdrup Technology, Inc., AEDC Group
Arnold Engineering Development Center
Arnold Air Force Base, TN 37389-6001

Walter O'Brien
Mechanical Engineering Department Head
Virginia Polytechnic Institute and State University
Blacksburg, VA 24061-0139

ABSTRACT

The direct approach of modeling the flow between all blade passages for each blade row in the compressor is too computationally intensive for practical design and analysis investigations with inlet distortion. Therefore a new simulation tool called the Turbine Engine Analysis Compressor Code (TEACC) has been developed. TEACC solves the compressible, time-dependent, 3D Euler equations modified to include turbomachinery source terms which represent the effect of the blades. The source terms are calculated for each blade row by the application of a streamline curvature code. TEACC was validated against experimental data from the transonic NASA rotor, Rotor 1B, for a clean inlet and for an inlet distortion produced by a 90-deg, one-per-revolution distortion screen. TEACC revealed that strong swirl produced by the rotor caused the compressor to increase in loading in the direction of rotor rotation through the distorted region and decrease in loading circumferentially away from the distorted region.

NOMENCLATURE

c_p	Constant pressure specific heat
E, F, G	Flux vectors
e	Internal energy and kinetic energy per mass
F	Component of force
F	Force
$\dot{m}$	Rate of mass flow
P	Pressure
Q	Conservation variables
R	Ideal gas constant
Residual	Vector representing the value of the explicit part of the implicit discretized conservation equations
r	Radial direction
S	Component of the source vector
S	Source vector
$\dot{SW}$	Rate of shaft work
T	Temperature
u	Velocity in the x-direction
V	Component of velocity
V	Velocity
$\forall$	Volume
v	Velocity in the y-direction
w	Velocity in the z-direction
x, y, z	Cartesian right-handed coordinate directions

Subscripts

b	Bleed
t	Total

INTRODUCTION

Modern high-performance military aircraft are subjected to rapid flight maneuvers which place great operational demands on their air-breathing gas turbine engines. One component of the engine that is particularly sensitive to the fluid dynamic transients that result from rapid aircraft maneuvers is the compressor. The compressor should operate in a stable manner during all aspects of flight. However, rapid flight

* The research reported herein was performed by the Arnold Engineering Development Center (AEDC), Air Force Materiel Command. Work and analysis for this research were performed by personnel of Virginia Polytechnic Institute and State University and by personnel of Sverdrup Technology, Inc., AEDC Group, technical services contractor for AEDC. Further reproduction is authorized to satisfy needs of the U. S. Government.

transients cause the inlet to produce a highly distorted total pressure flow field to the compressor inlet. High distortion levels may cause the compressor to surge at high rotational speeds or slip into rotating stall at lower rotational speeds (AIR-1419, 1983). Since total pressure distortion is the primary reason for reaching the engine stability limit, its effects on system performance and operability need to be understood.

Distortion imposed on a circumferentially swirling flow was shown by Greitzer and Strand (1978) to have a three-dimensional (3D) nature which is fundamental to the development of both inlets and compressors. Design or analysis engineers are interested in understanding the details of the flow field to determine the effects of inlet total pressure distortion on the compressor. One way to quantify the effects of distortion is to test for that effect in a ground test facility. Currently, the inlet and engine are tested separately. Typically, the aircraft fuselage is too big to fit in a wind tunnel. A forebody simulator is used in conjunction with the inlet to characterize its flow field. The forebody simulator is designed to produce a flow field at the inlet reference plane (IRP) similar to the flow field produced by the aircraft (Fig. 1).

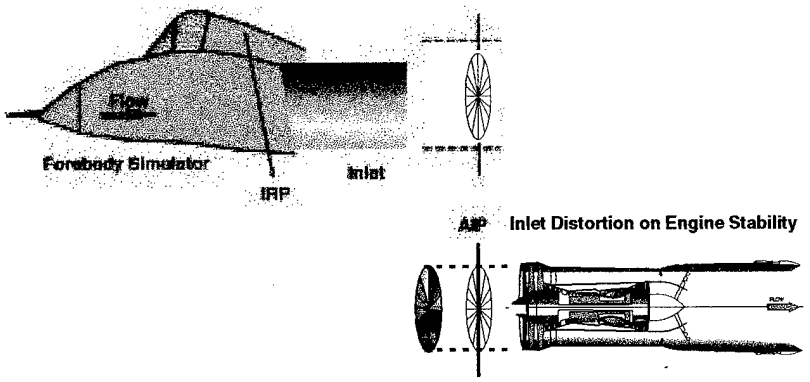

Fig. 1. Engine screen developed to duplicate distortion.

Screens are constructed to capture the most severe dynamic patterns produced by the inlet and are then placed in front of the engine to measure the loss of stall margin produced by the steady-state inlet distortion (AIR-1419, 1983). However, it is expensive to instrument a compressor and perform the necessary number of tests to adequately understand the compressor flow field. Therefore, numerical simulations have been developed to support the testing community.

Parallel compressor theory has been used successfully to develop an understanding of compressor performance with inlet distortion. Parallel compressor theory models the compressor with multiple circumferential segments and a uniform exit back boundary condition. Parallel compressor theory is restricted to simple inlet distortion patterns and is consistently conservative at estimating the stability limit. Investigators have made extensive modifications to parallel compressor theory through modeling techniques to account for the transfer of mass, momentum, and energy transfer between segments (Korn, 1974; Steenken, 1983; Mazzaway, 1977; Longley, 1992; Kimzey, 1977; Shahrokhi, 1995). 3D simulations have recently been developed which automatically account for the transfer of conservation properties (Billet, 1988; Tan, 1996). However, these investigations have been restricted to incompressible flow or low speed compression systems. There is still a need to develop a 3D compression system to investigate the effects of complex inlet distortion on a high speed compression system.

Therefore, a numerical simulation of inlet distortion has been developed and is called the **T**urbine **E**ngine **A**nalysis **C**ompressor **C**ode (TEACC). TEACC is a direct extension of previous work by the author (Hale, 1994) and solves the compressible three-dimensional (3D) Euler equations over a finite-volume grid domain through each blade row. The Euler equations are modified to include turbomachinery source terms which model the effect of the blades. The turbomachinery source terms are bleed, blade forces in the three Cartesian directions, and shaft work. The source terms are calculated for each circumferential grid section of each blade row by the application of a streamline curvature code. A methodology was developed for distributing the turbomachinery source terms axially, radially, and circumferentially through the bladed region.

OVERALL APPROACH TO TEACC

The overall TEACC development methodology is conceptually presented in Fig. 2. A general purpose 3D flow simulation computer code (NPARC, Cooper, 1989) is modified to accept turbomachinery source terms by semi-actuator disk theory. These turbomachinery source terms are calculated using a streamline curvature code (SLCC, Hearsey, 1970). TEACC is constructed by combining the technology of solving the Euler equations (NPARC) modified to include source terms and the technology of calculating the source terms (SLCC) to produce a time-dependent turbomachinery simulation with the capability of analyzing inlet distortion.

Governing Equations

The governing equations used in TEACC are developed by applying the conservation of mass, momentum, and energy. In turbomachinery flows, the viscous effects predominate mostly along the wall, making accurate simulation of the flow field away from the wall possible by using the Euler equations with turbomachinery source terms (Longley, 1992). The equations of fluid motion using the thermally and calorically perfect ideal gas assumption with turbomachinery source terms are:

$$\frac{\partial \mathbf{Q}}{\partial t}+\frac{\partial \mathbf{E}}{\partial x}+\frac{\partial \mathbf{F}}{\partial y}+\frac{\partial \mathbf{G}}{\partial z}=\mathbf{S}$$

$$e_t = e+\frac{1}{2}V^2 \qquad \mathbf{Q}=\begin{bmatrix}\rho\\ \rho u\\ \rho v\\ \rho w\\ \rho e_t\end{bmatrix}; \quad \mathbf{E}=\begin{bmatrix}\rho u\\ \rho u^2+P\\ \rho uv\\ \rho uw\\ \rho e_t+Pu\end{bmatrix}$$

$$\mathbf{F}=\begin{bmatrix}\rho v\\ \rho vu\\ \rho v^2+P\\ \rho vw\\ (\rho e_t+P)v\end{bmatrix}; \quad \mathbf{G}=\begin{bmatrix}\rho w\\ \rho wu\\ \rho wv\\ \rho w^2+P\\ (\rho e_t+P)w\end{bmatrix}; \quad \mathbf{S}=\begin{bmatrix}S_{\dot{m}}\\ S_{Fx}\\ S_{Fy}\\ S_{Fz}\\ S_{\dot{W}}\end{bmatrix}$$

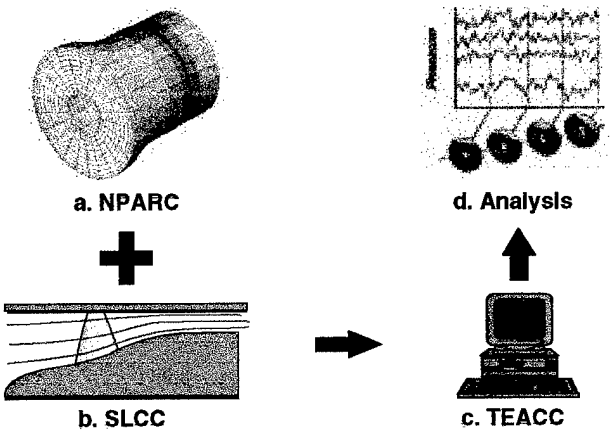

Fig. 2. Overall TEACC methodology.

The volumetric turbomachinery source terms are: (1) bleed per volume, (2) forces in the x, y, and z direction per volume, and (3) rate of shaft work per volume. The technique for calculating these source terms from the SLCC are developed later in this paper.

TEACC Boundary Conditions

The time dependent Euler equations with source terms define a hyperbolic in time and an elliptic in space system of equations requiring a full set of boundary conditions specified at all boundaries. The boundary conditions used with NPARC are explicit. The inflow boundary condition is based on reference plane characteristics, and the total pressure and total temperature at the inlet are specified. Inlet flow directions are assumed to be normal to the boundary. The exit boundary condition is a variable static pressure capable of supporting the exit profile of strong swirl. The exit static pressure is calculated by specifying a single value and imposing the static pressure profile of the adjacent upstream station on the exit. The wall boundary conditions are assumed to be slip wall; the normal velocity components are set equal to zero at the solid walls. A rotationally periodic (wrap-around) boundary condition is used in the circumferential direction, where the circumferential seam of the grid was overlapped by one circumferential segment.

TEACC Solution Procedure

TEACC's and NPARC's solution procedures are the same, solving the governing equations with the Beam and Warming approximate factorization algorithm (Beam, 1976) to obtain a flow-field solution. The above equations are consistently discretized with central differences to produce an implicit algorithm. The governing equations were cast in strong conservation form to keep global conservation, even if strong shocks are present. The technique of Pulliam and Steger (1980) to implement the Beam and Warming implicit algorithm was incorporated to diagonalize the implicit matrices, requiring a penta-diagonal solver. Since this is a central difference algorithm, artificial dissipation is included for stability. NPARC uses the Jameson-style (1981) improved shock-capturing artificial dissipation. TEACC, as well as NPARC, uses the time stepping method to achieve steady-state. There are two criteria used to verify TEACC's convergence to steady-state. First, the L2 norm of the residual is dropped to machine zero defined as:

$$\|\mathbf{Residual}\|_2 = \sqrt{\left(\sum_{q=1,n} \mathbf{Residual}_q^2\right)};$$

n = number of nodes. The second criteria used to verify TEACC's convergence to steady-state is to monitor key variables of interest and verify they no longer vary as TEACC continues to iterate.

TURBOMACHINERY SOURCE TERMS

Three-dimensional blade force and rate of shaft work terms are supplied by a streamline curvature code (SLCC). The SLCC is based on a radial redistribution of blade force and shaft work producing an "axisymmetric flow with swirl" in the form of streamlines. Necessary inputs include overall geometry, blade geometry, and loss and deviation correlations. These correlations are obtained from experimental data. A typical SLCC grid illustrated in Fig. 3 extends far upstream and far downstream of the compressor.

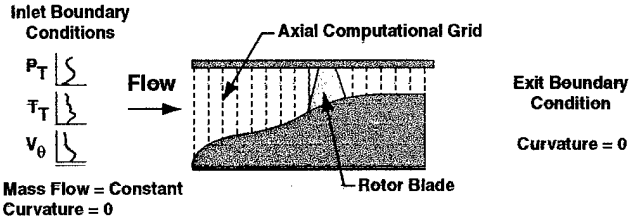

Fig. 3. Original SLCC with overall geometry.

Axial stations are chosen to include the inlet and exit of the blades and other convenient stations to allow a proper resolution of the flow field. Boundary conditions are required around the computational domain, with the outer casing and inner center-body treated as streamlines. The boundary conditions are inlet total pressure, inlet total temperature, and inlet swirl angle with curvature set equal to zero at both the inlet and exit. A particular operating point is established by specifying the rotor speed and overall mass flow.

The radial momentum equation was developed from the Euler equations by assuming that entropy and enthalpy do not change along streamlines except as prescribed across the blades by the loss and deviation correlations. The set of conservation equations are simplified by replacing the axial momentum and the energy equation with $\Delta S = 0$ and $\Delta H = 0$. The remaining two equations, continuity and radial momentum, are solved simultaneously at each axial station.

Modifications of the SLCC Technique

For the TEACC simulation to be responsive to the local change in total pressure due to inlet distortion and capable of modeling transients, the SLCC must be restricted to a small axial region on either side of the blades. Since the SLCC is a subsonic flow solver, it needs a full set of boundary conditions around its domain. The SLCC boundary conditions of inlet and exit curvature, overall mass flow, swirl angle, total

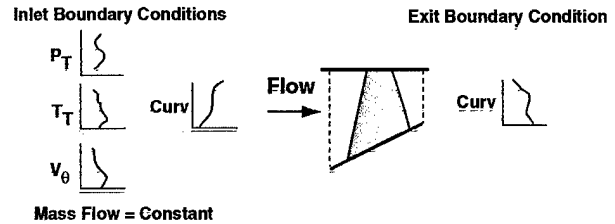

Fig. 4. Modifications to SLCC for calculating source terms.

temperature, and total pressure are calculated from the TEACC flow field. Fig. 4 is included to show the truncated grid in which the SLCC is restricted to operate.

Although the boundary conditions are of the same type in this new mode of operation as they were before the grid was truncated to the blades, they are now more complicated since they are no longer uniform but a function of the time dependent TEACC flow field around the blades.

The boundary conditions for the modified SLCC technique are outlined below for the computational domain specified in Fig. 4. Inlet and exit curvature provided by the 3D integrator are calculated from a circumferential projection of the flow field onto a circumferential slice (axial-radial plane). This is effectively the same as calculating streamline curvature from only the axial and radial velocity components of the 3D transient velocity flow field. Curvature is calculated as a function of local velocity and acceleration. Overall mass flow rate as a boundary condition to the SLCC is calculated from the 3D flow field just upstream of the bladed region by the integration of mass for each circumferential segment. The mass flow rate of each circumferential segment is summed together to calculate overall mass flow. A radial distribution of swirl angle is calculated from the TEACC solution at the blade inlet and defined as the arc-tangent of tangential velocity divided by axial velocity. The total temperature and total pressure at the inlet are calculated by using the conservation variables, ideal gas relations, and the compressible form of the stagnation definitions at the inlet of each control volume.

Technique to Calculate Turbomachinery Source Terms

The source term calculations are performed after the SLCC converges to a steady-state solution through the bladed region. The technique for calculating turbomachinery source terms uses control volumes within the bladed region and applies steady-state conservation laws across each control volume. Since the conservation of angular momentum is maintained in the axisymmetric solution of the SLCC, a radial distribution of circumferential velocity vectors are produced. Cartesian control volumes are constructed over a circumferential segment of the bladed region from streamlines and overall blade geometry with velocities and pressures known on all surfaces from streamline calculations. A simplifying assumption that the top and bottom surfaces of each control volume are streamsurfaces is incorporated since mass, momentum, and energy does not cross a streamsurface. The turbomachinery forces are calculated from a control volume analysis and the streamsurface assumption by the pressure area forces and the inertial forces (Fig. 5).

METHODOLOGY TO IMPLEMENT SOURCE TERMS INTO TEACC

With the TEACC-supplied boundary conditions, the SLCC produces an axisymmetric solution through the bladed region in the form of streamsurfaces which are constructed into control volumes to calculate turbomachinery source terms. A methodology for distributing the sources radially, circumferentially, and axially through the grid packed region through the blade was developed.

Radial Interpolation of Turbomachinery Source Terms

To implement these source terms into TEACC, a radial interpolation technique was derived. A radial distribution of sources is constructed by selecting the radius at the center of each SLCC source control volume (Fig. 6a). This radius is nondimensionalized by the radial extent of the inner and outer casing in the axial center of the blade (Fig. 6b).

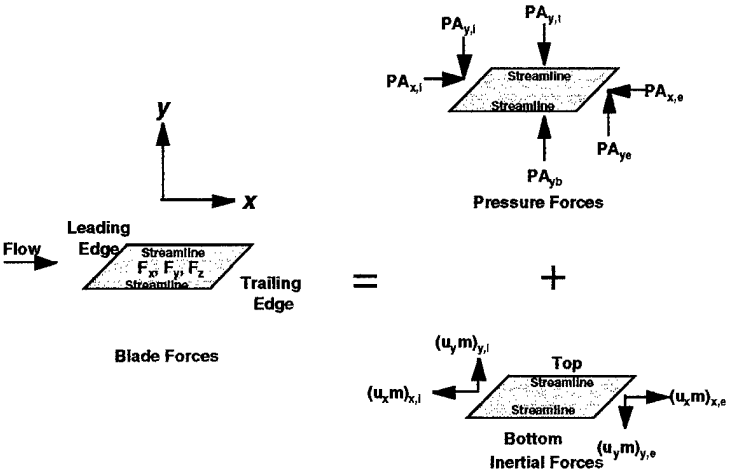

Fig. 5. Turbomachinery blade force calculations.

A spline is used to interpolate these source terms to TEACC along a single circumferential segment of the bladed region. A radial distribution of TEACC control volumes is defined through the bladed region using the existing grid structure as shown in Fig. 6c. The radius is nondimensionalized by the radial extent of the inner and outer casing in the middle of the bladed region. A radial distribution of TEACC source terms is acquired by interpolating the fixed TEACC volume centers onto the function of sources developed earlier from the SLCC as shown in Fig. 6d.

Circumferential Distribution of Turbomachinery Source Terms

The circumferential distribution of turbomachinery source terms are calculated by a direct application of the SLCC in each circumferential grid segment. For a distorted inlet upstream of the compressor, a circumferential inlet distortion is imposed on the system, as in Fig. 7a.

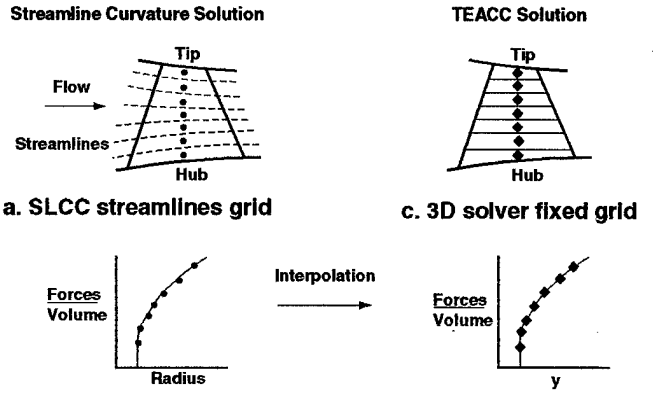

Fig. 6. Interpolation of radial distribution of source terms.

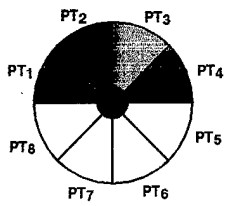

a. Circumferential distortion pattern

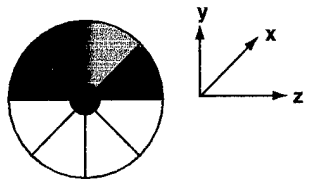

b. Distortion at the compressor inlet

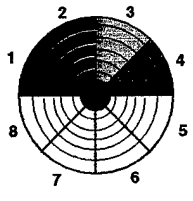

c. Streamline curvature solutions

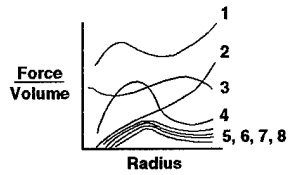

d. Interpolated source distribution

Fig. 7. Circumferential distribution of source terms.

This distortion affects the adjacent flow field, and Fig. 7b shows that this circumferential distortion, ignoring viscous effects, will persist up to the compressor inlet (Longley, 1992). The compressor's performance will be affected by this distortion, causing a nonuniform circumferential flow field. The modeling technique for acquiring a circumferential distribution of turbomachinery source terms applies the SLCC separately at each circumferential segment, as shown in Fig. 7c. The SLCC is sensitive to the changing demands to the flow field because it acquires its boundary conditions immediately upstream and downstream of each circumferential segment. Therefore, the SLCC interpolates a new radial distribution of turbomachinery source terms, sensitive to the changing flow field for each circumferential segment as shown in Fig. 7d. With a more complex inlet distortion pattern, the number of circumferential segments would be increased to maintain the high fidelity of the TEACC simulation.

Axial Distribution of Turbomachinery Source Terms

The grid was packed through the bladed region to reduce the numerical error from strong flow gradients. This method means a great deal of freedom exists in how the sources should be distributed through the bladed region. The sources are distributed conservatively through the bladed region by requiring that the sum of the sources distributed through the NPARC grid must equal the sum of the sources developed in the SLCC. A simple technique to investigate this problem was incorporated by using a weighting function which could take on a variety of linear shapes. However, a uniform weighting function was found to be the most robust.

VALIDATION RESULTS

Rotor 1B (Seyler, 1967) was chosen as the validation vehicle because it offered simplicity in the number of stages (1 blade row), and it represented a compression system with a thorough analysis of clean and distorted inlet. Rotor 1B is a high-performance transonic rotor similar to those found in modern high-speed aircraft. The rotor was designed with a multiple circular-arc blade shape which was applied over the top 40 percent of the blade while a double circular-arc construction was employed for the bottom 60 percent of the blade. With a hub-to-tip ratio at the rotor inlet of 0.5, the blade sections were long enough to require a mid-span damper to maintain structural integrity during operation. Rotor 1B consisted of 44 blades, producing a moderate solidity of 1.3 at the rotor tip.

Grid Development

TEACC requires a fixed three-dimensional grid on which to resolve the conservation equations. A grid of 69 × 13 × 26 was constructed to model Rotor 1B, where the inlet and exit of the blade were defined as slanting lines in Fig. 8. The grid was constructed with vertical grid lines in the vicinity of the screen to properly model the experimental distortion screen. Grid lines were smoothly packed to reduce numerical losses through the bladed region where the flow was known to have strong gradients. A radial-circumferential view of this base grid is presented in Fig. 9, where a cylindrical right-handed coordinate system has been used with uniform circumferential segments. An integer number of grid segments was constructed to conveniently model a 90-deg, one-per-revolution inlet distortion. Each segment was 15 degs in circumferential extent with a total of 24 segments within a circle (6 segments in each quadrant).

A grid density investigation was conducted by doubling the grid independently in each direction. This study revealed that the radial distribution of the flow field was unaffected by the increase in grid density. However, the error in overall total pressure ratio and efficiency was roughly halved by doubling the grid in the circumferential direction. This improvement was found to be directly related to halving the

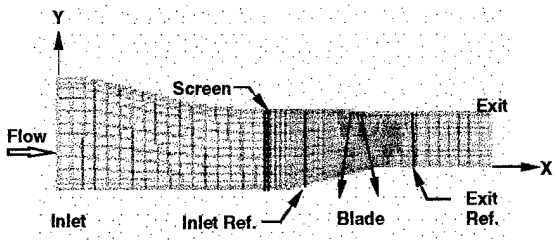

Fig. 8. Axial-radial view of 3D grid modeling Rotor 1B and test facility.

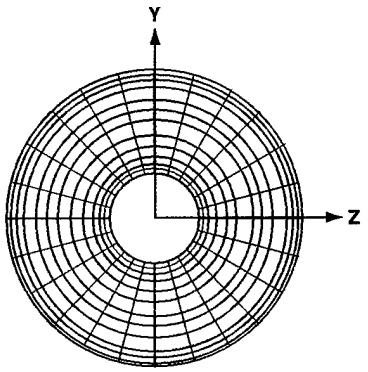

Fig. 9. Radial-circumferential view of 3D grid for Rotor 1B.

error in cross sectional area and mass flow by doubling the circumferential grid.

CLEAN INLET VALIDATION OF TEACC

TEACC was tailored to simulate Rotor 1B by calibrating the streamline curvature code (SLCC) used to calculate the turbomachinery source terms. The calibration was done by specifying a radial distribution of loss and exit relative flow angle from experimental data as a function of corrected mass flow and by specifying a radial distribution of blockage as a function of corrected mass flow.

Calculated overall total pressure map of Rotor 1B with a clean inlet is presented in Fig. 10 and compared with experimental data. Four corrected speeds (50, 70, 90, and 100 percent) were available for comparison, with symbols presented for the experimental data and lines for the TEACC solution. In an overall sense, there is good comparison between TEACC and data. The maximum percent difference in total pressure ratio is less than 1-percent difference for each characteristic.

TEACC's overall efficiency calculations for Rotor 1B are compared with experimental data in Fig. 11. The overall shape and character compares well with the experimental data. Each efficiency curve has a peak value which TEACC fails to reach, causing a maximum percent difference (for all speeds) between TEACC and experimental data of –2.9 percent occurring at the 50 percent corrected speedline.

Radial Comparison of TEACC with Data (Clean Inlet)

A radial comparison was made with exit total pressure and total pressure ratio as presented in Figs. 12 and 13 for the 100-percent speed point near the design throttle line. The overall shape is quite complicated for total pressure, increasing from hub to tip with the hub calculations deviating the most from experimental data by –1.3 percent. The tip and overall shape are in good agreement with the experimental data. The total pressure ratio is compared with data in Fig. 13, where a wide radial range in total pressure ratio can be seen. There is good agreement (1.0 percent difference) between TEACC and the experimental data. The exit static pressure and exit Mach number consistently support the strong distribution in total pressure ratio. As shown in Figs. 14 and 15, the exit Mach number and the exit static pressure are in good agree-

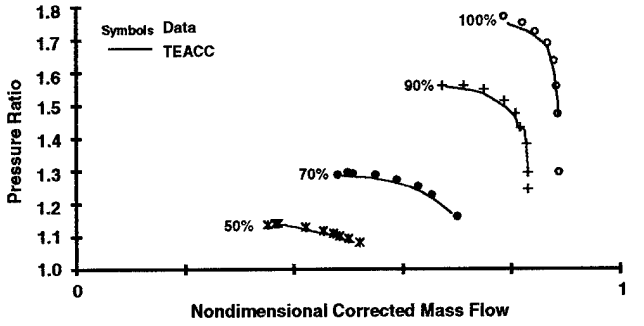

Fig. 10. Clean inlet, overall pressure ratio compared with experimental data.

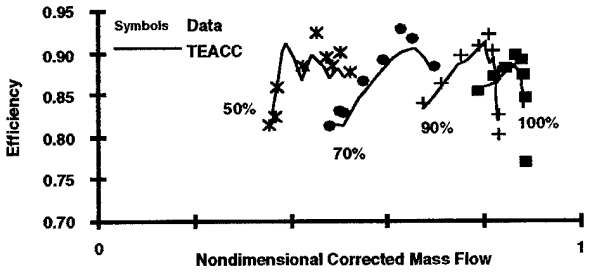

Fig. 11. Clean inlet, efficiency compared to experimental data.

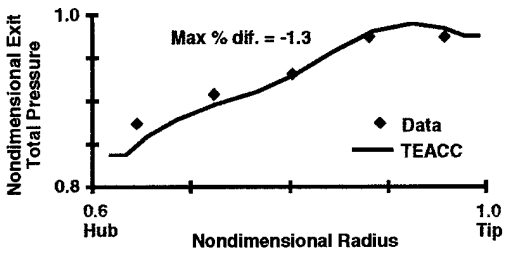

Fig. 12. Clean inlet, exit total pressure on the 100-percent speedline.

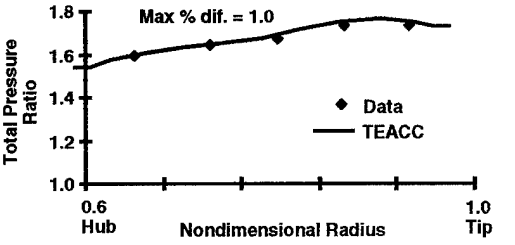

Fig. 13. Clean inlet, total temperature ratio on the 100-percent speedline.

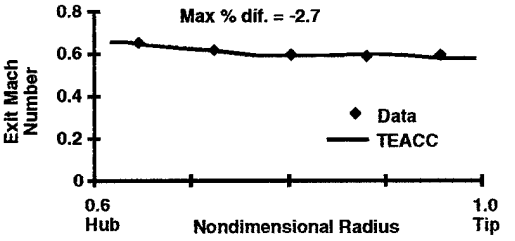

Fig. 14. Clean inlet, exit Mach number on the 100-percent speedline.

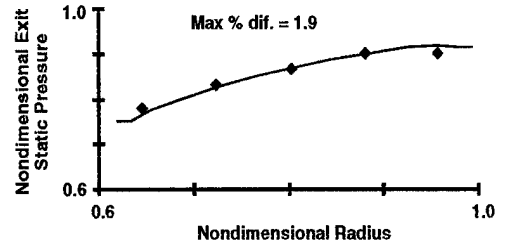

Fig. 15. Clean inlet, exit static pressure on the 100-percent speedline.

ment with the experimental data, and the exit Mach number is fairly uniform, but the exit static pressure varied consistent with the exit total pressure. The largest difference for both exit Mach number and exit static pressure with experimental data is at the tip, where Mach number is underpredicted by 2.7 percent and static pressure is overpredicted by 1.9 percent. The SLCC operates in the relative reference frame where the relative Mach number was observed to be transonic. The TEACC simulation remains in the absolute reference frame where Mach number remained subsonic (Fig. 14).

DISTORTED INFLOW VALIDATION OF TEACC

Rotor 1B was tested with an inlet screen to quantify the effects of inlet flow distortion on its performance. Because the distortion data provided with Rotor 1B was based on a 90-degree, one-per-revolution screen, a simulation of the screen was used in the TEACC simulation. For this study, TEACC was compared at three different corrected speedlines for a distorted inlet. A single distortion point on the 100-percent speedline was investigated in great detail because radial and circumferential data were available. Overall performance of the distorted compressor is compared to experimental data as well as radial and circumferential distributions.

Distortion Screen Modeling

To model the distortion screen, the porous wall boundary condition (Cooper, K., Jones, R., and Kincade, B. "NPARC Porous Wall Boundary Conditions." private communication and notes, May 1991; Pinker, 1967) was used. The boundary condition is semi-empirical in that experimental data has been taken across a variety of screens to establish a loss in total pressure as a function of Mach number, porosity, and Reynolds number. The value of total pressure at the exit of the screen was calculated from the continuity, energy equations (total enthalpy equal to a constant), and an empirical pressure loss coefficient. This general technique to simulate the effect of a distortion screen was incorporated for all inlet distortion calculations.

A single screen with a 90-deg, one-per-revolution pattern was designed to give a classical circumferential inlet total pressure inlet distortion to Rotor 1B. At the 100-percent speed, the experimental data showed that the screen produced a total pressure loss of 15 percent from the clean inlet which was duplicated for the TEACC simulation. Investigations were conducted through the middle of the four circumferential quadrants where the experimental data was taken. The screen was located in quadrant A (Fig. 16). The compressor rotates clockwise, causing air to swirl in the direction of increasing quadrant letter (A, B, C, and D).

Illustrated in Fig. 17 are the radial characteristics of the distortion screen simulation and comparison to experimental results

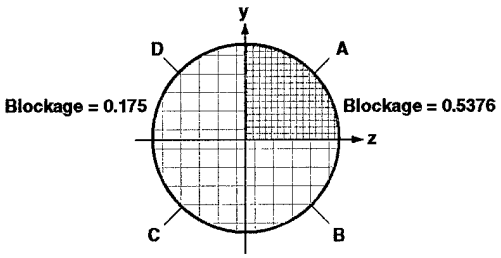

Fig. 16. Screen location and labeling.

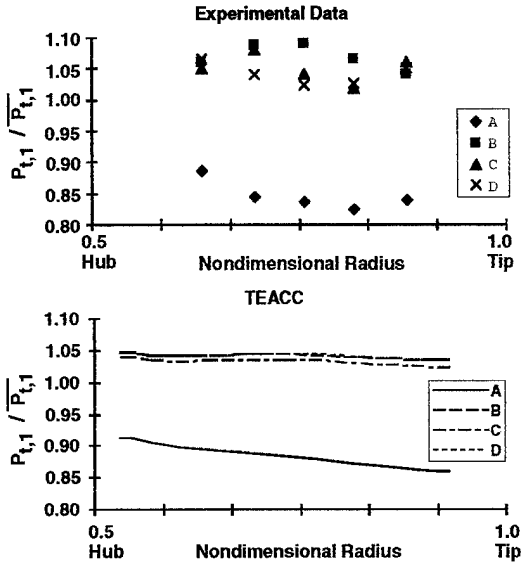

Fig. 17. Inlet total pressure distortion produced by the screen simulation at 100-percent corrected speed.

with experimental data in Fig. 17a and TEACC results in Fig. 17b. The character of the flow field behind the screen has certainly been captured, with Quadrant A (90-deg distortion) clearly separated from the other three quadrants. The individual pressure drops for Quadrants B-D calculated by the screen simulator are clustered together and represent the mean of the data in these quadrants. Not enough experimental data was available to adequately explain the scatter in the experimental data for Quadrants B-D. A possible explanation, however, is that the scatter is a result of unsteadiness in the flow field upstream of the distortion screen.

Overall Rotor 1B Performance Comparison (Distorted Inlet)

An overall total pressure ratio performance map for Rotor 1B is presented in Fig. 18 for three corrected speeds of 50, 70, and 100 percent. The clean speedlines are presented to give a proper orientation of the distorted data, with stall depicted for each speedline at its lowest corrected mass flow rate. A conservative, but simple, stalling criterion was imposed on the TEACC simulation. When any one of the circumferential segments acquired a corrected mass flow which exceeded stall

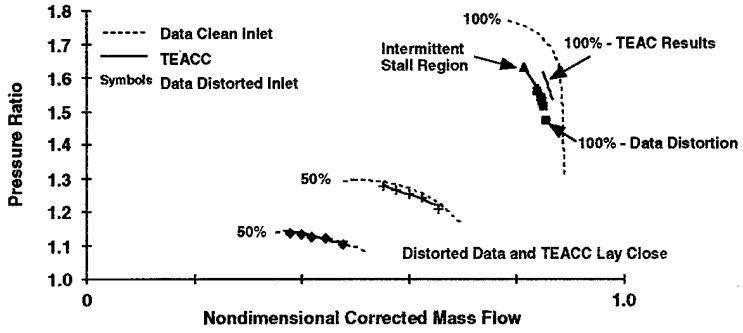

Fig. 18. Distorted Inlet, overall performance map with total pressure ratio at 100-percent corrected speed.

for the clean inlet, the compressor was considered stalled. Likewise, the TEACC simulation was halted when any one of the circumferential segments exceeded the clean inlet data on the choked end of the speedlines. These two restrictions define the distortion calculation limits presented for each speed in Fig. 18.

For the two low-speed cases, the clean and distorted data lay close together. The extent in corrected mass flow rate is about the same for the simulation and the experimental distortion data. The maximum percent difference between TEACC results and experimental data at the lower speeds was approximately 2 percent. The 100-percent speed is more interesting because the experimental data presented a region where the compressor intermittently stalled or remained stable with the imposed inlet distortion screen. The TEACC simulation predicted the corrected mass flow rate differently from reported experimental data by a maximum of 3 percent. The TEACC simulation maps out a range of corrected mass flow which includes approximately the middle of the intermittent stall region.

Overall efficiency is compared to experimental data in Fig. 19. In all cases TEACC predicts an efficiency that is higher than reported experimental data. The maximum percent difference between TEACC and the experimental data is located near the stall or choked portion of each corrected speed. The maximum percent difference between TEACC results and data are 6.9, 4.5, and 5.9 percent difference for 50-, 70-, and 100-percent speeds, respectively.

Radial Comparison of Compressor with Experimental Data (Distorted Inlet)

This investigation now turns to an examination of TEACC results compared to experimental data behind the compressor. Exit total pressure (defined by the ratio of exit total pressure over the average screen inlet total pressure) versus compressor radius is plotted with experimental data in Fig. 20a and TEACC results in Fig. 20b. Pressure ratio is characterized by a division between Quadrant A and the other three quadrants. TEACC does a good job of matching the character of the exit total pressure in Quadrant A with experimental data. TEACC results agree with the experimental data in the general character of the other three quadrants and identifies Quadrant B with the largest exit total pressure. The experimental data also confirms the TEACC results and shows that exit total pressure decreases steadily from Quadrant B to Quadrant D. Although the shapes of the other three quadrants are moving in the correct direction, the extent and scatter with pressure ratio is missing. The TEACC results in Quadrant A compare well to the experimental data, except for the hub point, which causes the maximum percent difference with pressure ratio equal to 6.15 percent. TEACC results compared to experimental data are too low for Quadrant B (6.82 percent) and too high for Quadrants C (5.86 percent) and D (8.64 percent). The highest maximum percent difference is within 8.7 percent in Quadrant D.

The final comparison with experimental data is also behind the compressor (same reference location as exit total pressure). The ratio of total temperature at the compressor exit divided by the average total temperature at the screen inlet is compared to experimental data with data presented in Fig. 21a and TEACC results in Fig. 21b. Quadrant A is again characterized as having a greater slope than the other three quadrants, and TEACC does a good job identifying this overall flow

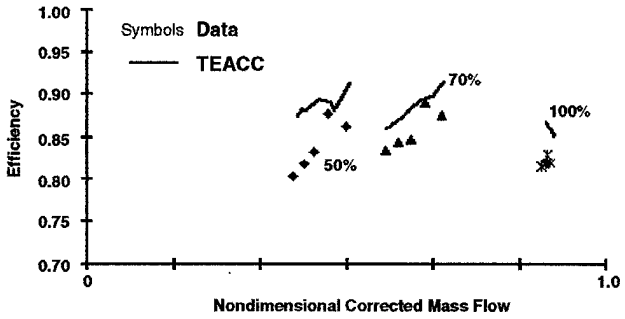

Fig. 19. Distorted inlet, overall performance map with efficiency.

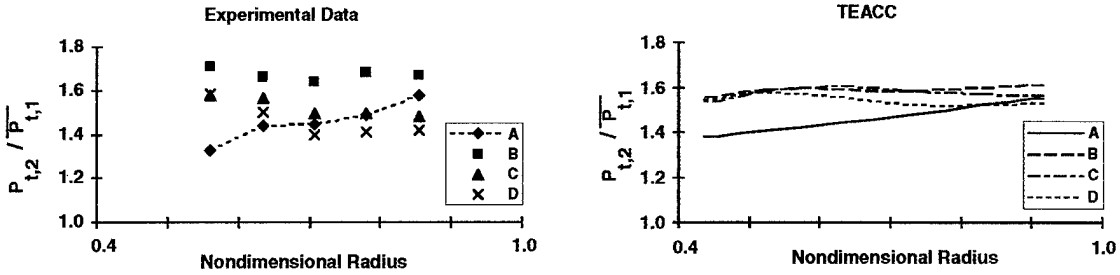

Fig. 20. Distorted inlet, exit total pressure on 100-percent speedline.

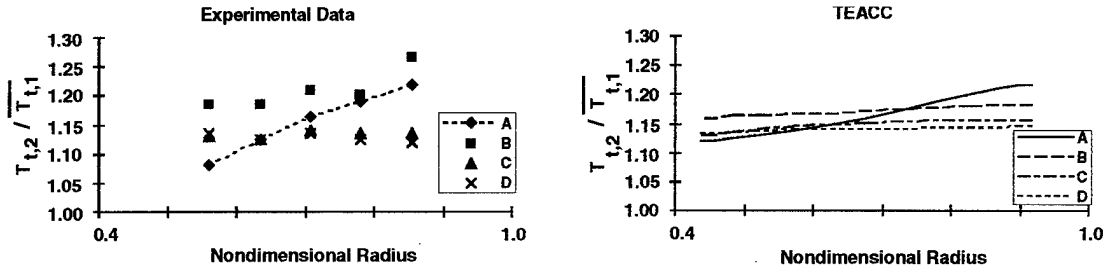

Fig. 21. Distorted inlet, exit total temperature on 100-percent speedline.

character. TEACC correctly identifies that, in the nondistorted region, the exit total temperature was the highest in Quadrant B, with the other quadrants decreasing in value from Quadrants B-D. TEACC's calculations for the total temperature at the compressor exit have a greater spread in Quadrants B-D than for the exit total pressure. Comparisons also show that the hub of Quadrant A is not as steep a slope as the experimental data, but the tip matches the data very well. Quadrants C and D match the data well, within 1.81 percent and 2.19 percent, respectively, and even Quadrant B matches the data well, except at a single tip point. The largest percent difference of TEACC with experimental data for exit total temperature is 6.60 percent.

EFFECT OF SWIRL ON THE COMPRESSOR PERFORMANCE WITH INLET DISTORTION

The circumferential velocity within the flow field caused by the high rotor speed compressor blade is a direct result of the compressor blade doing work on the flow. The blade causes a strong circumferential velocity which establishes the location of the largest static and total pressure regions. The compressor exit total pressure is presented in Fig. 22. Notice that the highest value in total pressure is not in the center of the distorted region, but has shifted clockwise and has its largest value near the tip. Displayed in Fig. 23 is exit total temperature, where it has shifted clockwise but is not as pronounced as the exit total pressure. Figure 24 presents the static pressure which resembles that of the previously presented total pressure. The highest static pressure is close to the interface of Quadrant A and B. The velocity vectors can be converted to streamlines which show the strong effect of swirl downstream of the compressor.

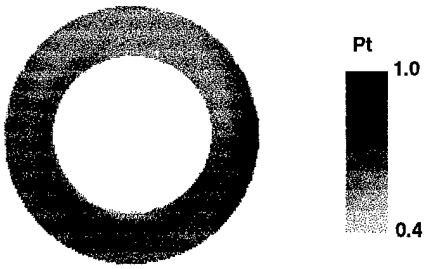

Fig. 22. Exit total pressure distribution produced by 90-deg, one-per-revolution screen on the 100-percent speedline.

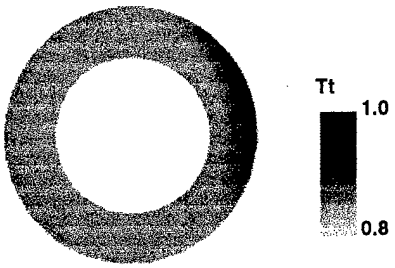

Fig. 23. Exit total temperature distribution produced by 90-deg, one-per-revolution screen on the 100-percent speedline.

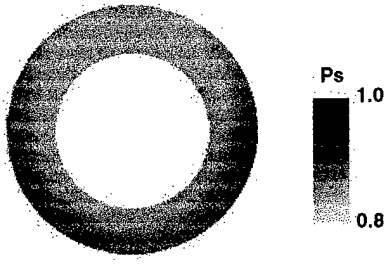

Fig. 24. Exit static pressure distribution produced by 90-deg, one-per-revolution screen on the 100-percent speedline.

The streamlines are shown in Fig. 25. A schematic of the distortion screen is presented to indicate inlet distortion (Fig. 25a); Quadrant A is defined in the middle of the distorted region and Segment D is chosen to represent a segment just before the rotor begins to sweep through the distortion in Quadrant D. An important distinction is that Quadrant A is in the distorted region, and Segment D is in the undistorted region. The upper right-hand picture in Fig. 25b shows in simple terms how Quadrant A and Segment D behave on the compressor map. First, Segment D operates in the clean inlet region of the compressor, producing a pressure ratio with a high corrected mass flow, but Quadrant A operates through the distorted screen where the total pressure in front of the compressor is low, causing a reduction in corrected mass flow. Quadrant A operates higher on the compressor map closer to stall, which means that approximately 75 percent of the compressor operates near choke while 25 percent of the compressor operates near stall. The portion of the compressor operating behind the distortion produces more work than any other part of the compressor.

The streamlines in the bottom view of Fig. 25c tell more about the compressor operation. Segment D describes the streamlines to the right of the distorted region while the blade turns the flow strongly toward and behind the distorted region. The streamlines through the middle of

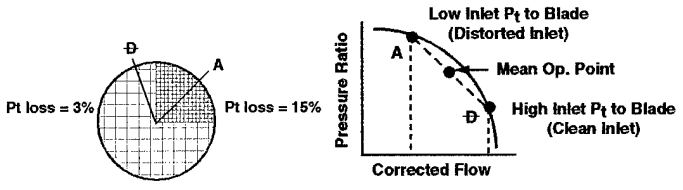

a. Distortion screen **b. Effect of inlet distortion**

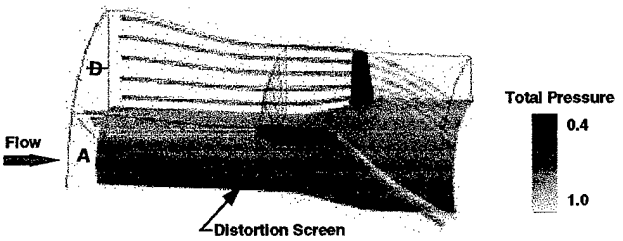

c. Streamlines through Rotor 1B

Fig. 25. Streamlines showing pressure convected with the flow on the 100-percent speedline with inlet distortion.

the distorted region are represented by Quadrant A. Again, the compressor strongly swirls the flow, but the total pressure increase through the distorted region is greater than that of Segment D. The flow field at the compressor exit is convected clockwise by the swirling flow to an adjacent part of the compressor, and the streamlines in Segment D show that the lower total pressure fluid is convected behind the compressor in the distorted region. This is a further indication of the clockwise transport of total pressure attributable to the swirling flow, and an indication that the total pressure behind the compressor is not uniform, but increasing in the direction of flow rotation. The performance increase which begins at the distorted region increases the static pressure behind the compressor and convects total temperature and total pressure with the flow to an adjacent point behind the compressor. This action causes the adjacent point to further backpressure the compressor in this region, subsequently increasing its performance and moving that region closer to stall. This increase implies that the swirl will cause the strongest backpressuring of the distorted region to be transported clockwise behind the adjacent non-distorted region (intersection of Quadrant A and B), increasing performance in this region and producing the largest total pressure found anywhere in the compressor, as shown in Fig. 22. Therefore, the total pressure increases clockwise through the distorted region.

The transport of total pressure and total temperature clockwise through the compressor can be viewed in a slightly different way through Fig. 26. Here, a radial mass-weighted average of total pressure and total temperature is presented versus the circumferential extent at the upstream and downstream reference locations. Inlet total pressure (Fig. 26b) to the compressor can be observed to have two different uniform regions, one behind the distortion screen (Quadrant A) and a higher value through the other three quadrants. The compressor exit total pressure increases steadily through the distorted region, with its highest value at the beginning of Quadrant B. The ratio of total pressure (Fig. 26a) also increases steadily in a clockwise direction through the distorted region, due to the compressor transportation of total pressure clockwise through the distorted region. This increases the static pressure behind an adjacent portion of the compressor in the clockwise direction, backpressuring this portion of the compressor and producing a performance increase. This increased performance shows itself as an increase in total pressure ratio.

A similar story can be constructed with total temperature at the compressor inlet and exit. The inlet total temperature to the compressor remains uniform in the presence of the screen, as shown in Fig. 26d. The exit total temperature, like the exit total pressure, steadily increases clockwise through the distorted region. This means the total temperature ratio in Fig. 26c also increases through the distorted region. Total temperature ratio, just like total pressure ratio, reaches its largest value at the interface of Quadrant A and Quadrant B because of the swirl effect through the distorted region.

SUMMARY/CONCLUSIONS

TEACC has been developed to model inlet distortion through the use of semi-actuator disk theory. This technique allows efficient computationalgridsthatprovideapracticalsolutionforinletdistortionproblems. TEACC was constructed by developing a methodology to merge two proven technologies, NPARC and a SLCC, into a single turbomachinery simulation.

TEACC's predictions with experimental data (Rotor 1B) for a clean inlet compared within 1 percent for total pressure ratio and within 3 percent difference for efficiency. A radial comparison of TEACC with experimental data also produced good results.

The distortion was produced with a 90-deg, one-per-revolution screen simulated by a boundary condition provided by NPARC. TEACC simulated Rotor 1B over three speedlines and produced a total pressure ratio which compared within 3 percent of experimental data and an efficiency which compared within 7 percent difference of experimental data.

A radial comparison of TEACC results to experimental data revealed that TEACC models the overall character of the compressor well and does a particularly good job of predicting the magnitude and shape of exit total temperature and exit total pressure in the distorted region (Quadrant A).

A detailed investigation of the compressor flow field was conducted to evaluate the effects of the distortion screen simulation and to compare these results with experimental data. The study revealed that strong swirl convects total temperature and total pressure with the flow in the direction of rotor rotation. This increase in total pressure produced an increase in static pressure in an adjacent part of the compressor which backpressured the compressor, producing an increase in performance. Therefore, the greatest total pressure is produced in transition from distorted to undistorted flow regions.

The TEACC development effort to simulate Rotor 1B with inlet distortion has been very successful. The TEACC technique was developed for a single Rotor and expected to be immediately expandable to multiple blade rows. TEACC is immediately recognized as a time dependent solution technique which can be extended to investigate surge and rotating stall instabilities. TEACC is an ideal environment to investigate inlet compatibility issues with the inlet and the compressor tightly coupled.

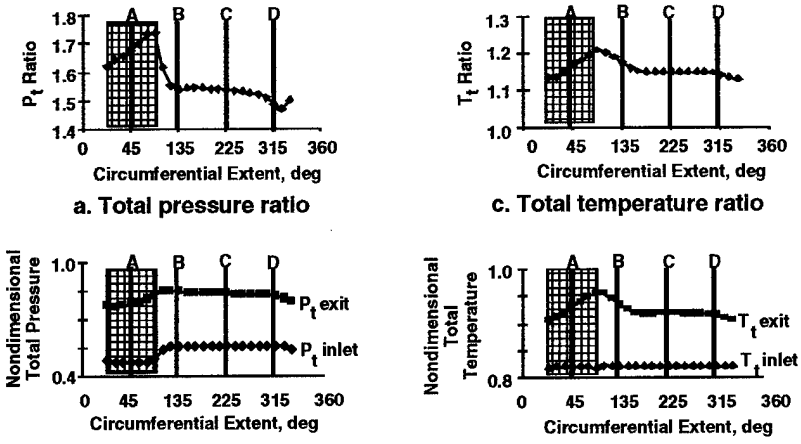

Fig. 26. Circumferential transport of total pressure and total temperature on 100-percent speedline.

REFFERENCES

Billet, G., Huard, J., Chevalier, P., and Laval, P. "Experimental and Numerical Study of the Response of an Axial Compressor to Distorted Inlet Flow." *Transactions of the ASME, Journal of Fluids Engineering*, Vol. 110, December 1988, pp. 355-360.

Cooper, G. K. and Sirbaugh, J. R. "PARC Code: Theory and Usage." AEDC-TR-89-15, December 1989.

Greitzer, E. M. and Strand, T. "Asymmetric Swirling Flows in Turbomachine Annuli." ASME-78-GT-109. ASME Gas Turbine Conference, London, England, April 1978.

Hale, A. A., Davis, M. W., Jr., and Kneile, K. R. "Turbine Engine Analysis Compressor Code: TEACC, Part I: Technical Approach and Steady Results." AIAA-94-0148. 32nd Aerospace Sciences Meeting, Reno, NV, January 1994.

Hearsey, R. M. "HT0300 - A Computer Program for the Design and Analysis of Axial Turbomachinery." Cambridge, MA, March 1970.

Jameson, A., Schmidt, W., and Turkel, E. "Numerical Solutions of the Euler Equations by Finite Volume Methods Using Runge-Kutta Time-Stepping Schemes." AIAA-81-1259. AIAA 14th Fluid and Plasma Dynamics Conference, Palo Alto, CA, 1981.

Kimzey, W. F. "An Analysis of the Influence of Some External Disturbances on the Aerodynamic Stability of Turbine Engine Axial Flow Fans and Compressors." AEDC-TR-77-80, August 1977.

Longley, J. P. and Greitzer, E. M. "Inlet Distortion Effects in Aircraft Propulsion System Integration." AGARD-LS-183. Advisory Group for Aerospace Research & Development Lecture Series, May 1992.

Mazzawy, R. S. "Multiple Segment Parallel Compressor Model for Circumferential Flow Distortion." *Transactions of the ASME, Journal of Engineering for Power*, April 1977, pp. 288-296.

Pulliam, T. H. and Steger, J. L. " Implicit Finite-Difference Simulations of Three Dimensional Compressible Flow." *AIAA Journal*, Vol. 18, No. 2, February 1980, pp. 159-167.

Seyler, D. R. and Gestolow, J. P. "Single Stage Experimental Evaluation of High Mach Number Compressor Rotor Blading Part 2- Performance of Rotor 1B." NASA-CR-54582, September 1967.

Shahrokhi, K. A. "Application of Modified Dynamic Compression System Model to a Low-Aspect Ratio Fan: Effects of Inlet Distortion." MS Thesis, Mechanical Engineering, Vanderbilt University, Nashville, TN, 1995.

Steenken, W. G. "Modeling Compression Component Stability Characteristics - Effects of Inlet Distortion and Fan Bypass Duct Disturbances." AGARD-CP-324. Advisory Group for Aerospace Research & Development Conference Proceedings, February 1983.

REPORT DOCUMENTATION PAGE

Form Approved
OMB No. 0704-0188

1. AGENCY USE ONLY *(Leave blank)*	2. REPORT DATE	3. REPORT TYPE AND DATES COVERED
	1997	Technical Society Paper, Aug. 1994 - Aug. 1997

4. TITLE AND SUBTITLE
A Three-Dimensional Turbine Engine Analysis Compressor Code (TEACC) for Steady-State Inlet Distortion

5. FUNDING NUMBERS
PR-0091

6. AUTHOR(S)
Alan Hale and Walter O'Brien

7. PERFORMING ORGANIZATION NAME(S) AND ADDRESS(ES)
Sverdrup Technology, Inc., AEDC Group
Arnold Engineering Development Center
Arnold AFB, TN 37389

8. PERFORMING ORGANIZATION REPORT NUMBER

9. SPONSORING/MONITORING AGENCY NAME(S) AND ADDRESS(ES)
AEDC/DOT
Arnold Engineering Development Center
Arnold AFB, TN 37389

10. SPONSORING/MONITORING AGENCY REPORT NUMBER

11. SUPPLEMENTARY NOTES
ASME 97-GT-124. Presented at ASME conference and to be published in the *Journal of Turbomachinery*.

12a. DISTRIBUTION AVAILABILITY STATEMENT
Approved for public release; distribution unlimited.

12b. DISTRIBUTION CODE
A

13. ABSTRACT *(Maximum 200 words)*
The direct approach of modeling the flow between all blade passages for each blade row in the compressor is too computationally intensive for practical design and analysis investigations with inlet distortion. Therefore a new simulation tool called the Turbine Engine Analysis Compressor Code (TEACC) has been developed. TEACC solves the compressible, time-dependent, 3D Euler equations modified to include turbomachinery source terms which represent the effect of the blades. The source terms are calculated for each blade row by the application of a streamline curvature code. TEACC was validated against experimental data from the transonic NASA rotor, Rotor 1B, for a clean inlet and for an inlet distortion produced by a 90-deg, one-per-revolution distortion screen. TEACC revealed that strong swirl produced by the rotor caused the compressor to increase in loading in the direction of rotor rotation through the distorted region and decrease in loading circumferentially away from the distorted region.

14. SUBJECT TERMS	15. NUMBER OF PAGES
compressor, turbomachinery, CFD, distortion	11
	16. PRICE CODE

17. SECURITY CLASSIFICATION OF REPORT	18. SECURITY CLASSIFICATION OF THIS PAGE	19. SECURITY CLASSIFICATION OF ABSTRACT	20. LIMITATION OF ABSTRACT
Unclassified	Unclassified	Unclassified	UL